Plantwide Fault Isolation Using Nonlinear Feedback Control

Benjamin J. Ohran,[†] Johnny Rau,[†] Panagiotis D. Christofides,*[,†,‡] and James F. Davis[†]

Department of Chemical and Biomolecular Engineering, University of California, Los Angeles, California 90095-1592, and Department of Electrical Engineering, University of California, Los Angeles, California 90095-1592

Accurate detection and isolation of faults is a critical component of a reliable and efficient plantwide fault-tolerant control system. In a recent work (Ohran et al. *AIChE J.* **2008**, *54*, 223), we demonstrated that using a nonlinear controller to enforce a specific structure in the closed-loop system allows data-based detection and isolation of certain faults that would otherwise not be isolable using data-based techniques that do not impose the necessary closed-loop system structure. In this work, it is demonstrated through a multiunit chemical process example how this approach can be applied in a plantwide setting. By using nonlinear, model-based control laws to decouple certain states from faults of interest, unique fault responses in the state trajectories are obtained in the closed-loop system. On the basis of the unique responses, fault isolation becomes possible using data-based statistical process monitoring methods. The effectiveness of the method was tested through an extensive Monte Carlo simulation study of 500 runs for each of four fault scenarios and through comparison with a conventional (proportional−integral) feedback control law.

1. Introduction

In the chemical process industry, process control system failures can lead to potentially catastrophic results that may jeopardize operator health and safety, the environment, and/or plant productivity. Past estimates of the economic impact of abnormal situations in the United States are in the range of tens of billions of dollars.[2] The potential consequences of control system failures are of particular significance in light of increased plant automation. While automation can increase operating efficiency, at the same time, reliance on automated systems increases susceptibility to control system failures. With such high costs associated with plant failures, it is now more important than ever that effective methods of failure detection and abnormal situation management be developed. Fault-tolerant control (FTC) is one method of dealing with process control system failures that has received a large amount of attention recently (see, for example, refs 3–6). FTC relies on redundant control system configurations that a plant supervisor can switch between in the presence of a fault.[7,8] In addition to redundant control configurations and a plant supervisor, implementation of a successful fault-tolerant control structure requires a fault detection and isolation (FDI) scheme.[9] The FDI scheme must accurately isolate the unit or units affected by the failure and must do so within a short enough time frame that the system is still within the controllability region of at least one of the remaining well-functioning control system configurations. Some of the major difficulties in performing successful fault detection and isolation stem from the fact that most chemical plants are highly nonlinear and often have fully coupled dynamics. This makes process behavior hard to predict and state responses to different faults generally indistinguishable.

Methods of fault detection based on process measurements as developed in the field of statistical process monitoring are fairly reliable and accurate for detecting the presence of a fault.[10–12] However, fault isolation is a more difficult task. Generally, fault isolation techniques are divided into two categories: model-based and data-based. Model-based techniques rely on a mathematical model of the process to create dynamic filters and compute residuals that directly relate to specific faults. Using the model-based approach, fault isolation can be performed for specific model and fault structures.[9,13–15] These methods are usually based on a deterministic process model that must be fairly accurate to function effectively. On the other hand, data-based methods of fault detection and isolation rely exclusively on process measurements. For fault detection, data are used to create thresholds for normal operation based on historical measurements under fault-free behavior. In general, data-based methods of fault isolation require historical data obtained from the system under faulty behavior in order to distinguish between faults. This is accomplished by comparing the current system location in the state space with the known regions of the state space and/or fault directions during faulty operation. Other methods have been developed that consider the contribution of particular states to the overall shift from normal operation.[16] Many data-based methods take advantage of principle component analysis (PCA) to more effectively handle large amounts of data or to find relationships within the data.[17,18] It is also common to group data based on process subsystems or process distinct timescales as in multiblock or multiscale PCA.[19–21] While these methods have had varying degrees of success, isolation remains a difficult task, particularly for nonlinear systems when historical data under faulty operation are hard to obtain or are insufficient to discriminate between faults. For a comprehensive review of model-based and data-based fault detection and isolation methods, the reader may refer to refs 22 and 23. While both model-based and data-based approaches to fault detection and isolation have received significant attention by the research community, methods that use principles from both areas have received little attention.

The focus of this work is to demonstrate in a plant-wide setting a recently introduced method of fault detection and isolation that integrates model-based controller design with data-based fault detection in order to perform fault isolation. In ref 1, we demonstrated how a model-based controller could be designed to enhance the isolability of particular faults in the closed-loop system. In this approach, specific faults are partially

* Corresponding author. E-mail: pdc@seas.ucla.edu.
[†] Department of Chemical and Biomolecular Engineering, University of California.
[‡] Department of Electrical Engineering, University of California.

10.1021/ie071548i CCC: $40.75
Published on Web 05/28/2008

decoupled from other states in the system in order to create a unique response for individual faults in the system. Data-based process monitoring techniques are used to detect the presence of a fault and to allow isolation based upon the enforced structure within the closed-loop system. The method is demonstrated using a multiunit process consisting of a two continuous stirred tank reactor (CSTR) system and a flash tank separator with recycle. The study demonstrates that the achievement of fault isolation across multiple coupled units is possible through feedback control. Additionally, the effects of process and sensor measurement noise on the ability to detect and accurately isolate faults are investigated through a Monte Carlo simulation study. The results from the nonlinear control simulation were compared with a conventional (proportional−integral) feedback controller to demonstrate that, without the isolable structure induced by feedback control, the faults are otherwise indistinguishable without prior knowledge of fault history.

2. Preliminaries

2.1. Fault Signatures. The objective of this paper is to demonstrate the method proposed in ref 1 of controller-enhanced fault detection and isolation in a multiunit setting. Controller enhanced FDI was introduced in ref 1 as a method of dividing the state vector into a number of partially decoupled subvectors that can be monitored for their individual responses to particular faults in the system using process measurements only. On the basis of their responses and the system structure imposed by the model-based controllers, it is possible to discriminate between individual faults or groups of faults. Dividing the state vector into partially decoupled subvectors is accomplished by using model-based control laws to enforce an appropriate structure. On the basis of this structure, faults affecting the system produce a unique response as observed in the state trajectories. The responses of the subvectors are monitored for out-of-control behavior using standard process monitoring methods that take into account the acceptable level of variation under normal operating conditions (i.e., common cause variation). Thus, this approach brings together model-based controller design techniques and data-based statistical process monitoring for diagnosing faults. To better understand the structure that must be enforced in order to perform fault isolation, we review the definitions of the incidence graph, the reduced incidence graph, and the isolability graph[1] in the context of nonlinear deterministic systems.

2.1.1. Definition 1. The incidence graph of an autonomous system $\dot{x} = f(x)$ with $x \in \mathbb{R}^n$ is a directed graph defined by n nodes, one for each state, x_i, $i = 1, ..., n$, of the system. A directed arc with origin in node x_i and destination in node x_j exists if and only if $\partial f_j/\partial x_i \neq 0$.

2.1.2. Definition 2. The reduced incidence graph of an autonomous system $\dot{x} = f(x)$ with $x \in \mathbb{R}^n$ is the directed graph of nodes q_i, where $i = 1, ..., N$, that has the maximum number of nodes, N, and satisfies the following conditions:

• To each node q_i there corresponds a set of states $X_i = \{x_j\}$. These sets of states are a partition of the state vector of the system, i.e., $\cup X_i = \{x_1, ..., x_n\}$, $X_i \cap X_j = \emptyset$, $\forall i \neq j$.

• A directed arc with origin q_i and destination q_j exists if and only if $\partial f_l/\partial x_k \neq 0$ for some $x_l \in X_i$, $x_k \in X_j$.

• There are no loops in the graph.

The incidence graph of a system shows the time derivative dependencies between the states. By reducing fully coupled states to a single node, the reduced incidence graph reveals any partially decoupled subsystems that may exist. With the structure of the subsystems revealed, it is beneficial to look at how faults affect each of the subsystems as shown in an isolability graph.

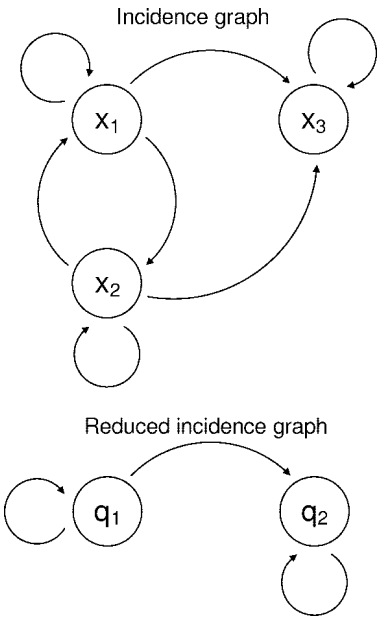

Figure 1. Incidence and reduced incidence graphs for the system of eq 1.

2.1.3. Definition 3. The isolability graph of an autonomous system $\dot{x} = f(x, d)$ with $x \in \mathbb{R}^n$, $d \in \mathbb{R}^p$ is a directed graph made of the N nodes of the reduced incidence graph of the system $\dot{x} = f(x, 0)$ and p additional nodes, one for each possible fault d_k. The graph contains all the arcs of the reduced incidence graph of the system $\dot{x} = f(x, 0)$. In addition, a directed arc with origin in fault node d_k and destination to a state node q_j exists if and only if $\partial f_l/\partial d_k \neq 0$ for some $x_l \in X_j$.

These definitions are convenient in presenting the basic dependencies within a state vector. Although this graphical approach has the advantage of visualizing the system structure, it may be noted that it is also possible to understand and express to some extent the structure of a system and its faults using the notion of relative degree.[24] This approach has been used previously in other FDI works.[1,9]

In most complex systems, the states are fully coupled and the isolability graph contains a single node representing all of the states in the system. However, in systems with partially decoupled dynamics, this demonstrates graphically the partially independent subsets of the state vector. Consider, for example, the following system:

$$\begin{aligned} \dot{x}_1 &= x_1 + x_2 + u + d_1 \\ \dot{x}_2 &= -x_2 + x_1 + d_2 \\ \dot{x}_3 &= x_1 - x_2 - x_3 + d_3 \end{aligned} \tag{1}$$

Figure 1 shows the incidence and reduced incidence graphs for the system of eq 1. Because x_1 and x_2 are mutually dependent but are not affected by x_3, they form a partially decoupled subsystem represented by a single node (q_1) in the reduced incidence graph, leaving x_3 to form a node by itself (q_2). Figure 2 shows the effect of each of the faults in the isolability graph for the system of eq 1.With the isolability graph of a system, it is possible to consider fault isolation based upon monitoring of the subsystems. For this purpose, it is necessary to review the definition of a fault signature given below.[1]

2.1.4. Definition 4. The signature of a fault d_k of an autonomous system subject to p faults $\dot{x} = f(x, d)$ with $x \in \mathbb{R}^n$, $d \in \mathbb{R}^p$ is a binary vector $\mathbf{W}^k$ of dimension N, where N is the

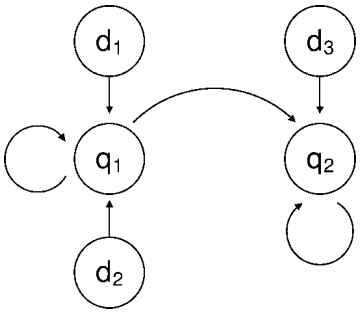

Figure 2. Isolability graph of the system of eq 1.

number of nodes of the reduced incidence graph of the system. The ith component of $\mathbf{W}^k$, denoted W_i^k, is equal to 1 if there exists a path in the isolability graph from the node corresponding to fault k to the node q_i corresponding to the set of states X_i; W_i^k is equal to 0 otherwise.

Using this definition of a fault signature and the isolability graph shown in Figure 2, it is possible to identify the fault signatures for the three faults considered in the system of eq 1. In this case, because the node $q_2 = \{x_3\}$ does not affect the node $q_1 = \{x_1, x_2\}$, the fault d_3 has the signature $W^3 = [0\ 1]$ and the two faults d_1 and d_2, which affect q_1 and q_2, have the signature $W^1 = W^2 = [1\ 1]$. On the basis of this, it is expected that a failure in d_1 or d_2 will affect all of the states, whereas a failure in d_3 is expected to affect only those in q_2 . In this regard, it is possible to distinguish a failure in d_3 from a failure in d_1 or d_2 based on the system response. However, it is not generally possible to discriminate between a failure in d_1 and d_2.

2.1.5. Remark 1. The process model for the system of eq 1 does not explicitly account for process and sensor noise. Likewise, the isolability graph and the associated fault signatures are developed for the deterministic case. However, noise is accounted for in the process monitoring method given in the next section by means of appropriate tolerance thresholds (computed using historical process data) in the decision criteria for fault detection and isolation. The thresholds are based on historical, fault-free operating data and take into account both sensor and process noise present under normal operating conditions. This allows for appropriate FDI performance even if the process model and the measurements are corrupted by noise.

2.2. Process Monitoring. The discussion in the previous subsection focused on deterministic process behavior in which evaluation of the fault signature based on the isolability graph is straightforward. On the other hand, in processes subject to state and measurement noise, it is possible to have false positives and false negatives in determining the effect of a fault on the state trajectories. In the Simulation Results section of this paper, autocorrelated noise is added to the process dynamic equations and white sensor noise is added to the process measurements. For this reason, in order to make a comparison between the fault signature based on the expected response of the system from the isolability graph and the system signature based on the actual behavior (computed on the basis of process measurements), it is necessary to use a method of monitoring the state trajectories that clearly distinguishes normal behavior from faulty behavior and is tolerant to the normal amount of process variation (as computed from process historical data). Additionally, it is assumed that faults of interest will be sufficiently large so that their effect will not be masked by normal process variation; faults whose influence on the closed-loop system behavior over a large time window is within the normal common-cause process variation do not have a significant effect on the process. These types of faults are generally inconsequential and do not need to be handled via fault-tolerant control schemes.

For the purpose of process monitoring, we use Hotelling's T^2 statistic, a well-established method in statistical process control that monitors multivariate data using a single statistic.[25] Because of its suitability for continuous, serially correlated chemical processes, the method of using single observations is employed.[26,27] The T^2 statistic is computed using the multivariate state vector (or subset of the state vector) $x \in \mathbb{R}^n$, the expected or desired mean $\bar{x}$ (the normal operating point) and the estimated covariance matrix $\mathbf{S}$ obtained using h historical measurements of the system under normal operation:

$$T^2 = (x - \bar{x})^{\mathrm{T}} \mathbf{S}^{-1} (x - \bar{x}) \tag{2}$$

The upper control limit for the T^2 statistic is obtained from its distribution and is computed using the following equation:

$$T_{\mathrm{UCL}}{}^2 = \frac{(h^2 - 1)n}{h(h - n)} F_\alpha(n,\ h - n) \tag{3}$$

where $F_\alpha(n, h - n)$ is the value from the F distribution with $(n, h - n)$ degrees of freedom corresponding to a confidence level α. The T^2 statistic is used to both detect that a fault has occurred as well as provide the system signature that can be compared with the fault signatures defined by the isolability graph. In order to perform these tasks, the T^2 statistic based on the full state vector $\mathbf{x}$ with upper control limit $T_{\mathrm{UCL}}{}^2$ is first used to detect the presence of a fault. Subsequently, the T_i^2 statistic is used to monitor the status of each subset of the state vector with an upper control limit $T_{\mathrm{UCL}i}{}^2$ where $i = 1, ..., N$ that is based on each of the nodes q_i and their corresponding states $x_j \in X_i$.

The fault detection and isolation procedure then follows the steps given below:[1]

(1) A fault is detected if $T^2(t) > T_{\mathrm{UCL}}{}^2\ \forall t,\ t_\mathrm{f} \le t \le T_\mathrm{P}$ where t_f is the first time T^2 crosses the UCL and T_P is chosen so that the window $T_\mathrm{P} - t_\mathrm{f}$ is large enough to allow fault isolation with a desired degree of confidence. Choosing T_P depends on the process time constants and potentially on available historical information on the process behavior.

(2) A fault that is detected can be isolated if the signature vector of the fault $W(t_\mathrm{f}, T_\mathrm{P})$ can be built as follows:

$$T_i^2(t) > T_{\mathrm{UCL}i}{}^2 \quad \forall\, t \quad t_\mathrm{f} \le t \le T_\mathrm{P} \rightarrow W_i(t_\mathrm{f}, T_\mathrm{P}) = 1$$

$$T_i^2(t) \text{ not greater than } T_{\mathrm{UCL}i}{}^2 \quad \forall\, t \quad t_\mathrm{f} \le t \le T_\mathrm{P} \rightarrow W_i(t_\mathrm{f}, T_\mathrm{P}) = 0$$

In such a case, fault d_k is detected at time T_P if $W(t_\mathrm{f}, T_\mathrm{P}) = \mathbf{W}^k$. If two or more faults are defined by the same signature, isolation between them is not possible on the basis of the fault signature obtained from the isolability graph.

It should be noted that the method of fault detection discussed here makes no assumption regarding the time variation of the fault. In general, both abrupt and slowly developing faults will be detected and isolated. However, slowly developing faults are more likely to be subject to false isolation if the fault is diagnosed before becoming sufficiently large, as discussed in Remark 2. To minimize such effects, it is important to adjust the detection window T_P, based on the individual system dynamics. The reader may refer to refs 28–30 for more discussion on this issue. Additionally, it should be noted that the detection and isolation method discussed here requires no significant real-time computation other than computing the T^2 statistics, which require only minimal computation time.

2.2.1. Remark 2. In the data-based fault detection and isolation method presented above, the upper control limit is chosen based on common-cause variance, including process and sensor noise, in order to minimize false alarms. Additionally, to further avoid false alarms, a period of persistent failure is required, $T_P - t_f$. For these reasons, small disturbances or failures are likely to go undetected if the magnitude and effect of the disturbance is on the same level as that of the inherent process variance. Specifically, in order to declare a fault, d_k must be sufficiently large in order for $T_i^2(t)$ to exceed the threshold T_{UCLi}^2 $\forall t$, $t_f \le t \le T_P$. Clearly, faults that do not meet the criteria for declaring a fault are, from the point of view of faulty behavior, not of major consequence. However, it should be noted that there is the probability (albeit low) that there is a fault d_k that is large enough to signal a fault in the full-state vector, **x**, but is not large enough to signal a fault in all of the affected subgroups. In this case, it is possible to have a false isolation. This is investigated in the results section by simulating the closed-loop system a large number of times with randomly varying fault sizes in a Monte Carlo type simulation.

2.3. Controller Design. The approach to fault detection and isolation discussed in the previous two sections can be applied if the signatures of the faults in the closed-loop system are distinct. The uniqueness of a fault depends on the structure of the closed-loop system as shown in the isolability graph. In general, complex nonlinear systems are fully coupled and faults cannot be isolated using this method when the controller is designed only with closed-loop stability in mind. Despite this being the case for most open-loop systems, an isolable structure in the closed-loop system can still be achieved through the application of appropriately designed nonlinear control laws. Although many control laws exist that will achieve the desired goal, it is not possible to apply a systematic procedure to controller design that guarantees closed-loop stability and an isolable closed-loop system structure for any nonlinear process. The specific form of the controller depends on the structure of the open-loop system and it is possible that such a controller may not exist. Nonetheless, a general approach can be applied to decouple a particular set of states from the rest of the system in a number of applications. As an example, consider a controller that can be applied to nonlinear systems with the following state-space description:

$$\begin{aligned} \dot{x}_1 &= f_{11}(x_1) + f_{12}(x_1, x_2) + g_1(x_1, x_2)u + d_1 \\ \dot{x}_2 &= f_2(x_1, x_2) + d_2 \end{aligned} \tag{4}$$

where $x_1 \in R$, $x_2 \in \mathbb{R}^n$, $u \in \mathbb{R}$, and $g_1(x_1, x_2) \neq 0$ for all $x_1 \in R$, $x_2 \in \mathbb{R}^n$. With a nonlinear state feedback controller of the form

$$u(x_1, x_2) = -\frac{f_{12}(x_1, x_2) - v(x_1)}{g_1(x_1, x_2)} \tag{5}$$

the closed-loop system takes the form

$$\begin{aligned} \dot{x}_1 &= f_{11}(x_1) + v(x_1) + d_1 \\ \dot{x}_2 &= f_2(x_1, x_2) + d_2 \end{aligned} \tag{6}$$

where $v(x_1)$ has to be designed in order to achieve asymptotic stability of the origin of the x_1 subsystem when $d_1 = 0$. In this case, the proposed controller guarantees asymptotic stability of the closed-loop system, as well as different signatures for faults d_1 and d_2 . Note that the reduced incidence graph is defined by two nodes corresponding to both states and the signatures are given by $W^1 = [1\ 1]^T$ and $W^2 = [0\ 1]^T$. If necessary, using multiple controllers allows for more degrees of freedom in breaking up the full-state vector into subvectors.

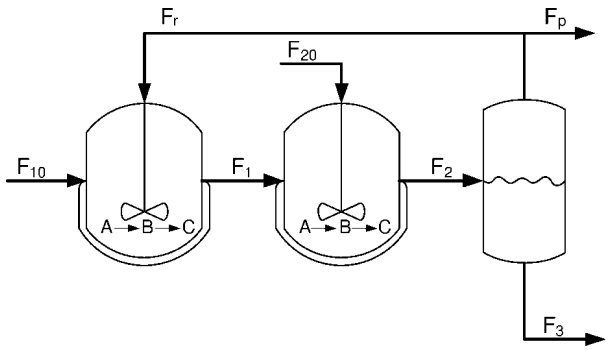

Figure 3. Reactor−separator system with recycle.

As an example, this is demonstrated with the system of eq 1. Consider a controller added to the right-hand side of the dynamic equation for the state x_1 of the form:

$$u = -x_2 + v$$

where v is an external controller that may be used for stabilizing the system. With this controller, the closed-loop system takes the following form:

$$\begin{aligned} \dot{x}_1 &= x_1 + d_1 + v \\ \dot{x}_2 &= -x_2 + x_1 + d_2 \\ \dot{x}_3 &= x_1 - x_2 - x_3 + d_3 \end{aligned} \tag{7}$$

Since there are no longer loops in the system, the reduced incidence graph is now equivalent to the incidence graph having three nodes (one for each state). Consequently, it becomes possible to distinguish between faults d_1 and d_2 in addition to d_3 using the method described above. This method will be applied to the reactor−separator system described in the next section. Note that the controller design outlined above does not take into consideration optimality criteria beyond the tuning of the external controller v . It is likely that the nonlinear feedback control law that enforces an isolable structure will incur additional cost compared with a control law designed for optimality. In the Simulation Results section, this issue is addressed by comparing the nonlinear feedback controller with a conventional proportional−integral (PI) controller to show that the cost incurred for enabling fault isolation in the closed-loop system is not excessive.

2.3.1. Remark 3. It is important to note that it is possible to extend the state feedback controller design to an output feedback controller design, which uses a high-gain observer operating at a fast time-scale to achieve state estimation, to enforce a near-isolable structure in the closed-loop system. The reader may refer to refs 31–33 for results on high-gain observer-based output feedback control. However, the detailed development of this approach is outside of the scope of the present work.

3. Reactor−Separator Process

3.1. Process Description and Modeling. The process considered in this study is a three-vessel, reactor−separator system consisting of two continuously stirred tank reactors (CSTRs) and a flash tank separator (see Figure 3). A feed stream to the first CSTR contains reactant A, which is converted into the desired product B . The desired product can then further react into an undesired side-product C . The effluent of the first CSTR along with additional fresh feed makes up the inlet to the second CSTR. The reactions A → B and B → C (referred to as 1 and 2, respectively) take place in the two CSTRs in series before the effluent from CSTR 2 is fed to a flash tank. The overhead

Table 1. Process Variables

x_{A1}, x_{A2}, x_{A3}	mass fractions of A in vessels 1, 2, and 3
x_{B1}, x_{B2}, x_{B3}	mass fractions of B in vessels 1, 2, and 3
x_{C1}, x_{C2}, x_{C3}	mass fractions of C in vessels 1, 2, and 3
x_{Ar}, x_{Br}, x_{Cr}	mass fractions of A, B, and C in the recycle
T_1, T_2, T_3	temperatures in vessels 1, 2, and 3
T_{10}, T_{20}	feed stream temperature to vessels 1 and 2
F_1, F_2, F_3	effluent flow rate from vessels 1, 2, and 3
F_{10}, F_{20}	feed stream flow rate to vessels 1 and 2
F_r, F_p	flow rates of the recycle and purge
V_1, V_2, V_3	volume of vessels 1, 2, and 3
u_1, u_2	manipulated inputs
E_1, E_2	activation energy for reactions 1 and 2
k_1, k_2	pre-exponential values for reactions 1 and 2
ΔH_1, ΔH_2	heats of reaction for reactions 1 and 2
α_A, α_B, α_C	relative volatilities of A, B, and C
Q_1, Q_2, Q_3	heat input into vessels 1, 2, and 3
C_p, R	heat capacity and gas constant

vapor from the flash tank is condensed and recycled to the first CSTR, and the bottom product stream is removed. A small portion of the overhead is purged before being recycled to the first CSTR. All three vessels are assumed to have static holdup. The dynamic equations describing the behavior of the system, obtained through material and energy balances under standard modeling assumptions, are given below.

$$\frac{dx_{A1}}{dt} = \frac{F_{10}}{V_1}(x_{A10} - x_{A1}) + \frac{F_r}{V_1}(x_{Ar} - x_{A1}) - k_1 e^{\frac{-E_1}{RT_1}} x_{A1}$$

$$\frac{dx_{B1}}{dt} = \frac{F_{10}}{V_1}(x_{B10} - x_{B1}) + \frac{F_r}{V_1}(x_{Br} - x_{B1}) + k_1 e^{\frac{-E_1}{RT_1}} x_{A1} - k_2 e^{\frac{-E_2}{RT_1}} x_{B1}$$

$$\frac{dT_1}{dt} = \frac{F_{10}}{V_1}(T_{10} - T_1) + \frac{F_r}{V_1}(T_3 - T_1) + \frac{Q_1}{\rho C_p V_1} + \frac{-\Delta H_1}{C_p} k_1 e^{\frac{-E_1}{RT_1}} x_{A1} + \frac{-\Delta H_2}{C_p} k_2 e^{\frac{-E_2}{RT_1}} x_{B1} + u_1$$

$$\frac{dx_{A2}}{dt} = \frac{F_1}{V_2}(x_{A1} - x_{A2}) + \frac{F_{20}}{V_2}(x_{A20} - x_{A2}) - k_1 e^{\frac{-E_1}{RT_2}} x_{A2}$$

$$\frac{dx_{B2}}{dt} = \frac{F_1}{V_2}(x_{B1} - x_{B2}) + \frac{F_{20}}{V_2}(x_{B20} - x_{B2}) + k_1 e^{\frac{-E_1}{RT_2}} x_{A2} - k_2 e^{\frac{-E_2}{RT_2}} x_{B2}$$

$$\frac{dT_2}{dt} = \frac{F_1}{V_2}(T_1 - T_2) + \frac{F_{20}}{V_2}(T_{20} - T_2) + \frac{Q_2}{\rho C_p V_2} + \frac{-\Delta H_1}{C_p} k_1 e^{\frac{-E_1}{RT_2}} x_{A2} + \frac{-\Delta H_2}{C_p} k_2 e^{\frac{-E_2}{RT_2}} x_{B2} + u_2$$

$$\frac{dx_{A3}}{dt} = \frac{F_2}{V_3}(x_{A2} - x_{A3}) - \frac{F_r + F_p}{V_3}(x_{Ar} - x_{A3})$$

$$\frac{dx_{B3}}{dt} = \frac{F_2}{V_3}(x_{B2} - x_{B3}) - \frac{F_r + F_p}{V_3}(x_{Br} - x_{B3})$$

$$\frac{dT_3}{dt} = \frac{F_2}{V_3}(T_2 - T_3) + \frac{Q_3}{\rho C_p V_3} \tag{8}$$

The definitions for the variables used in eq 8 can be found in Table 1, with the parameter values given in Table 2. Each of the tanks has an external heat input. In both CSTRs, the heat input is a manipulated variable for controlling the reactors at the appropriate operating temperature. These are the only control actuators considered in the system. The model of the flash tank separator operates under the assumption that the relative volatility for each of the species remains constant within the operating temperature range of the flash

Table 2. Parameter Values

$T_{10} = 300$, $T_{20} = 300$	K
$F_{10} = 1.4 \times 10^{-3}$, $F_{20} = 1.4 \times 10^{-3}$	m^3/s
$F_r = 1.4 \times 10^{-2}$, $F_p = 1.4 \times 10^{-3}$	m^3/s
$V_1 = 1.0$, $V_2 = 0.5$, $V_3 = 1.0$	m^3
$E_1 = 5 \times 10^4$, $E_2 = 6 \times 10^4$	J/mol
$k_1 = 2.77 \times 10^3$, $k_2 = 2.5 \times 10^3$	1/s
$\Delta H_1 = -6 \times 10^4$, $\Delta H_2 = -7 \times 10^4$	J/mol
$C_p = 4.2 \times 10^3$	J/kg K
$R = 8.314$	J/mol K
$\rho = 1000$	kg/m^3
$Q_1 = 3.5 \times 10^5$, $Q_2 = 4.5 \times 10^5$, $Q_3 = 3.5 \times 10^5$	J/s
$\alpha_A = 3.5$, $\alpha_B = 1$, $\alpha_C = 0.5$	unitless

tank. This assumption allows for calculating the mass fractions in the overhead based upon the mass fractions in the liquid portion of the vessel. It has also been assumed that there is a negligible amount of reaction taking place in the separator. The following algebraic equations model the composition of the overhead stream relative to the composition of the liquid holdup in the flash tank:

$$x_{Ar} = \frac{\alpha_A x_{A3}}{\alpha_A x_{A3} + \alpha_B x_{B3} + \alpha_C x_{C3}}$$

$$x_{Br} = \frac{\alpha_A x_{B3}}{\alpha_A x_{A3} + \alpha_B x_{B3} + \alpha_C x_{C3}}$$

$$x_{Cr} = \frac{\alpha_A x_{C3}}{\alpha_A x_{A3} + \alpha_B x_{B3} + \alpha_C x_{C3}} \tag{9}$$

The open-loop system of eq 8 is fully coupled and is represented by a single node in the reduced incidence graph. However, by using appropriately designed model-based nonlinear state feedback control laws for the manipulated inputs u_1 and u_2, it is possible to separate the closed-loop system into four nodes in the isolability graph. Consider the following nonlinear control laws that decouple the full-state vector into four subvectors,[33]

$$u_1 = \frac{F_r}{V_1}(T_{3ss} - T_3) - \frac{-\Delta H_1}{C_p} k_1 e^{\frac{-E_1}{RT_1}}(x_{A1} - x_{A1ss}) - \frac{-\Delta H_2}{C_p} k_2 e^{\frac{-E_2}{RT_1}}(x_{B1} - x_{B1ss}) + v_1$$

$$u_2 = -\frac{-\Delta H_1}{C_p} k_1 e^{\frac{-E_1}{RT_2}}(x_{A2} - x_{A2ss}) - \frac{-\Delta H_2}{C_p} k_2 e^{\frac{-E_2}{RT_2}}(x_{B2} - x_{B2ss}) + v_2 \tag{10}$$

where the subscript ss refers to values at the steady state, or set point. The terms v_1 and v_2 are external controllers used to stabilize the system and achieve offset-free output tracking and are defined, according to standard proportional−integral control formulas, as follows:

$$v_1(t) = K_1\left(T_{1ss} - T_1 + \frac{1}{\tau_{I1}}\int_0^t (T_{1ss} - T_1)\, dt\right)$$

$$v_2(t) = K_2\left(T_{2ss} - T_2 + \frac{1}{\tau_{I2}}\int_0^t (T_{2ss} - T_2)\, dt\right) \tag{11}$$

where K_1 and K_2 are the proportional controller gains and τ_{I1} and τ_{I2} are the integral time constants. The closed-loop system operating under the control laws defined in eqs 10 and 11 decouples T_1 from x_{A1}, x_{B1} and T_3 and T_2 from x_{A2}, x_{B2} . The four subgroups created by the controller of eqs 10 and 11 are $q_1 = \{T_1\}$, $q_2 = \{T_2\}$, $q_3 = \{T_3\}$ and $q_4 = \{x_{A1}, x_{A2}, x_{A3}, x_{B1}, x_{B2}, x_{B3}\}$. The resulting isolability graph is shown in Figure 4. From the isolability graph, the fault signatures can be defined as follows:

$$W^1 = [1;\ 1;\ 1;\ 1]$$

$$W^2 = [0;\ 1;\ 1;\ 1]$$

$$W^3 = [0;\ 0;\ 1;\ 0]$$

$$W^4 = [0;\ 0;\ 0;\ 1] \quad (12)$$

The four faults shown in Figure 4 are those that will be considered in this example. They represent failures in the heat inputs to each of the tanks (faults d_1, d_2, and d_3) and a feed stream concentration disturbance in species A in the inlet to CSTR 1 (d_4). These are added to the right-hand side of the dynamic equations for T_1, T_2, T_3, and x_{A1} . Note that the FDI approach used places no restrictions on the fault d_i, which can represent any time-varying signal. Thus, faults may be additive or parametric and can represent any fault (e.g., time-varying biases, actuator failures, disturbances, process parameter failures). When a fault in the control actuator occurs that makes the actuator unusable (i.e., where $d = -u$), then the imposed feedback closed-loop system structure breaks down, resulting in a fault signature of the closed-loop system that is different from the one under fault-free operation, and thus making the isolation of such a fault possible.

For comparison purposes, in the simulation results, a PI controller with the form given in eq 11 is used. This control law is used for comparing the isolability of faults, using process measurements only, in the closed-loop system under PI-only control and in the closed-loop system under the nonlinear feedback control which enforces the isolable structure. Although a PI controller is used for comparison in this work, any controller that does not enforce an isolable structure in the closed-loop system would yield similarly indistinguishable faults. Additionally, the PI-only controller will be used to evaluate the additional cost incurred by the nonlinear feedback controller in order to enforce an isolable structure in the closed-loop system.

3.2. Simulation Results. The model presented in Section 3.1 was numerically simulated using a standard Runge−Kutta integration method. The system was modeled with both process and sensor noise. The sensor measurement noise was generated as Gaussian distributed random noise with standard deviation σ_m and was added to the state measurement at a sample rate of 0.1 sample/s. Noisy measurements were used in updating the feedback control law described in eqs 10 and 11 on the same interval. Process noise was added to the right-hand side of each equation in the system of ordinary differential equations (ODEs) found in eq 8. Process noise was generated as autocorrelated noise of the form $w_k = \varphi w_{k-1} + \xi_k$, where $k = 0$, 1, etc. is the discrete time step of 1 s, w_k is a normally distributed random variable with standard deviation σ_p, and φ is the autocorrelation factor. Table 3 contains the parameters used in generating the noise. The sensor measurement and process noise were generated independently for each state in the system. For purposes of fault detection, a window of 30 s was used in declaring a fault (i.e., $T_P - t_f = 30$ s).

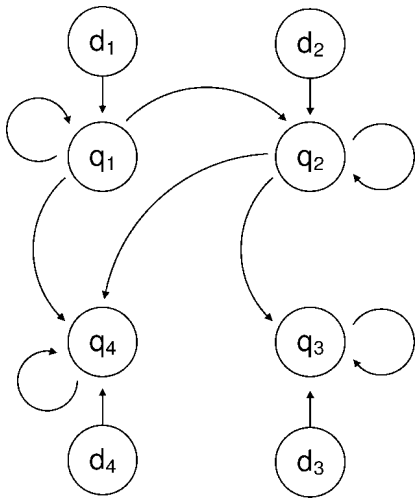

Figure 4. Isolability graph for the reactor−separator system.

Table 3. Noise Parameters

	σ_m	σ_p	φ
x_{A1}	1×10^{-3}	1×10^{-3}	0.7
x_{B1}	1×10^{-3}	1×10^{-3}	0.7
T_1	1×10^{-3}	1×10^{-2}	0.7
x_{A2}	1×10^{-3}	1×10^{-3}	0.7
x_{B2}	1×10^{-3}	1×10^{-3}	0.7
T_2	1×10^{-3}	1×10^{-2}	0.7
x_{A3}	1×10^{-3}	1×10^{-3}	0.7
x_{B3}	1×10^{-3}	1×10^{-3}	0.7
T_3	1×10^{-3}	1×10^{-2}	0.7

The controllers were designed as shown in eqs 10 and 11 using control parameters $K_1 = K_2 = 0.01$ s^{-1} and $\tau_{I1} = \tau_{I2} = 300$ s . The PI controllers shown for comparison used the same parameters. The system was controlled at the set-point values of $T_{1ss} = 436.8$ K and $T_{2ss} = 433.9$ K . In all cases, the system was initially at steady state and was simulated for 30 min fault-free and for 30 min after the occurrence of the fault. The four faults were introduced as added terms on the right-hand side of the ODEs in eq 8; only a single fault was applied in each simulation. The values $d_1 = 1$ K/s, $d_2 = 2$ K/s, $d_3 = 1$ K/s, and $d_4 = -2 \times 10^{-3}$ s^{-1} were added to the dynamic equations for T_1, T_2, T_3, and x_{A1}, respectively. These represent changes in the heat input (actuator/valve failures) for faults d_1, d_2, and d_3 and an inlet concentration disturbance in species A for fault d_4. However, these faults could also be thought of as any general faults because the development of this method does not limit the values that d can take.

Four simulation scenarios were carried out, one for each fault, to demonstrate the method of detecting and isolating faults in the closed-loop system. In order to apply the method of fault detection and isolation presented in Section 2, the data should be multivariate normal and fit the T^2 distribution under closed-loop operation. Figure 5 demonstrates that the measurements from each of the states closely approximates a Gaussian distribution. The distribution for the measured T^2 values is

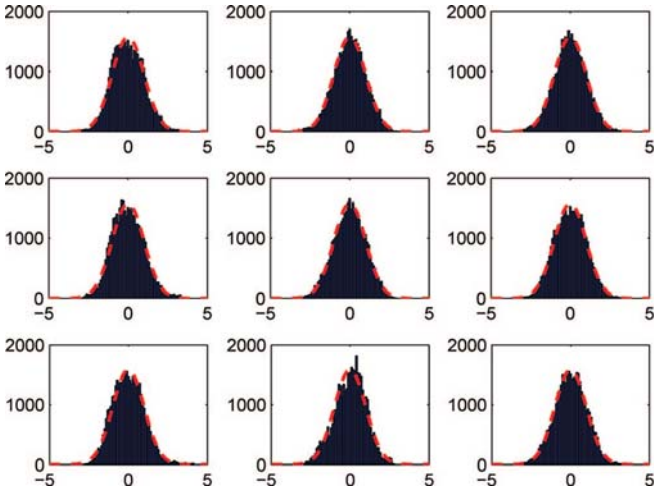

Figure 5. Normalized histogram plots of each of the system states compared with a normal distribution (dashed) for a large number of measurements during fault-free operation under nonlinear feedback control.

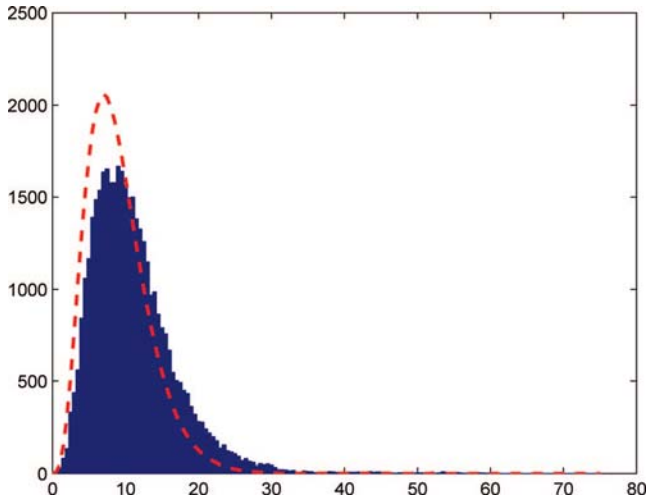

Figure 6. Histogram of T^2 statistic for the full-state vector compared with the expected T^2 distribution (dashed) for a large number of measurements during fault-free operation under nonlinear feedback control.

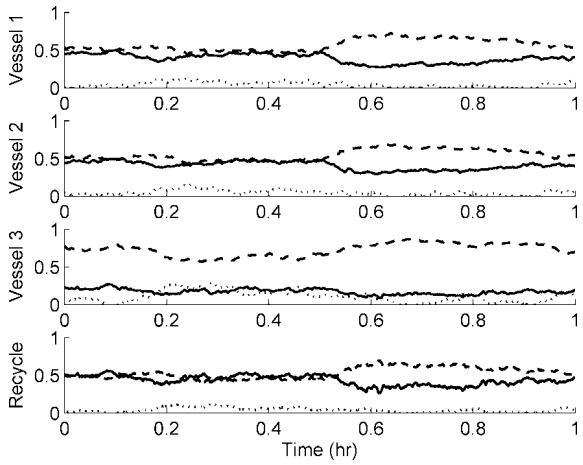

Figure 7. Plots of the mass fractions x_A (solid), x_B (dashed), and x_C (dotted) for the system under nonlinear feedback control with a failure in d_1 at $t = 0.5$ h.

shown in Figure 6. Again we see that the measured statistic closely approximates the predicted distribution; however, in this case, the fit is less exact because of correlation between states. Nonetheless, the distribution is reasonably close. If necessary, the upper control limit can be adjusted upward to provide a more conservative limit if false alarms are a problem.

Figure 7 shows the trajectories of the mass fractions in each of the tanks and the recycle stream for the simulation in closed-loop operation under the nonlinear feedback controller with a failure in d_1. The effects of the failure at time $t = 0.5$ h are visible in the plot. The temperature trajectories for each of the tanks are shown in Figure 8 along with the control action requested. Once the failure is detected at $t = 0.5$ h, the T_i^2 plots are used to determine the fault signature for the system. Figure 9 shows the T^2 statistic results for the four subsets of the state vector as well as for the full-state vector. The fault is detected at time $t = 0.5$ h by the full T^2 and is isolated based on the four T_i^2 corresponding to the subsets. On the basis of the T_i^2 plots, the signature of the system in this case is $W = [1; 1; 1; 1] \equiv W^1$. Thus, the fault is correctly isolated as one affecting the states in $q_1 = T_1$ or d_1 . Note that, although the process data are serially correlated on a short time scale, this was compensated for by using a large amount of historical data for estimating $\mathbf{S}$. Additionally, it has been found that feedback control makes the closed-loop system data more normally distributed (see ref 27).

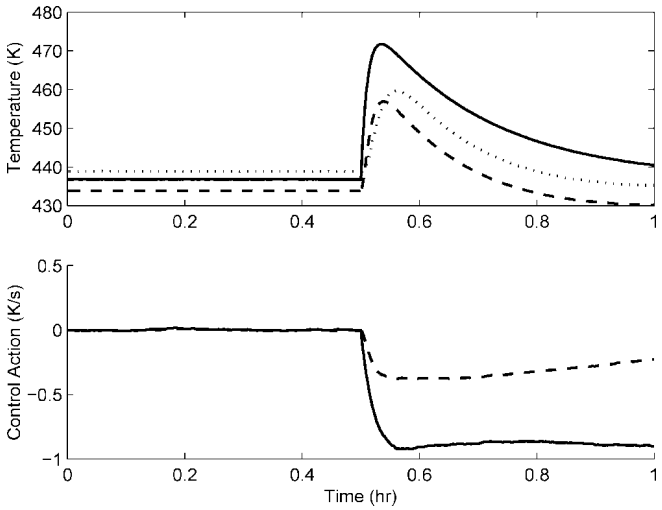

Figure 8. (top) Temperature trajectories for T_1 (solid), T_2 (dashed), and T_3 (dotted) for the system under nonlinear feedback control with a failure in d_1 at $t = 0.5$ h. (bottom) Control action requested for the same system for u_1 (solid) and u_2 (dashed).

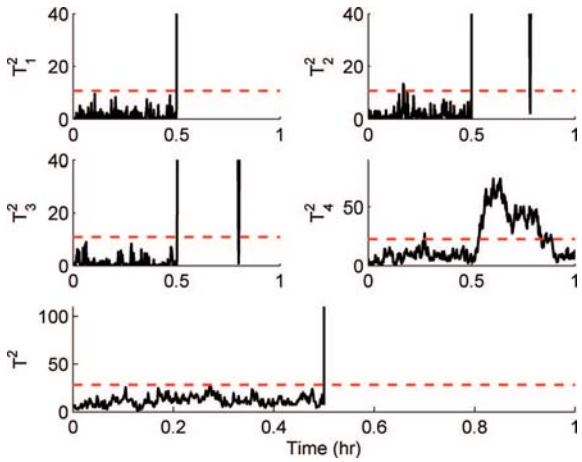

Figure 9. Plots of the T^2 statistic (solid) with the corresponding T_{UCL}^2 (dashed) for each of the subsystems and for the full-state vector under nonlinear feedback control with a failure in d_1 at $t = 0.5$ h.

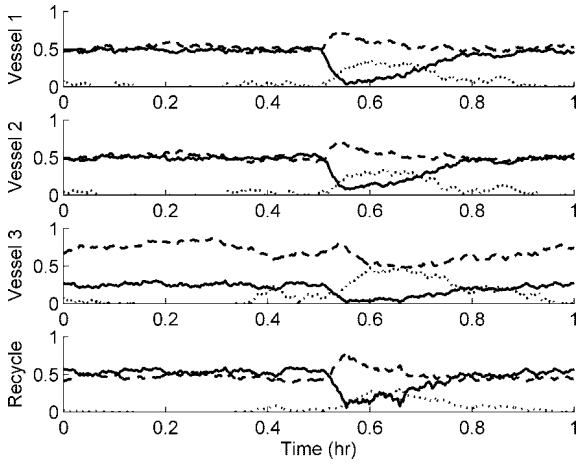

Figure 10. Plots of the mass fractions x_A (solid), x_B (dashed), and x_C (dotted) for the system under PI control with a failure in d_1 at $t = 0.5$ h.

Thus, the assumption that the data are multivariate normal for applying the T^2 statistic is reasonable. This was also confirmed in Figures 5 and 6. The simulation with a failure in d_1 was

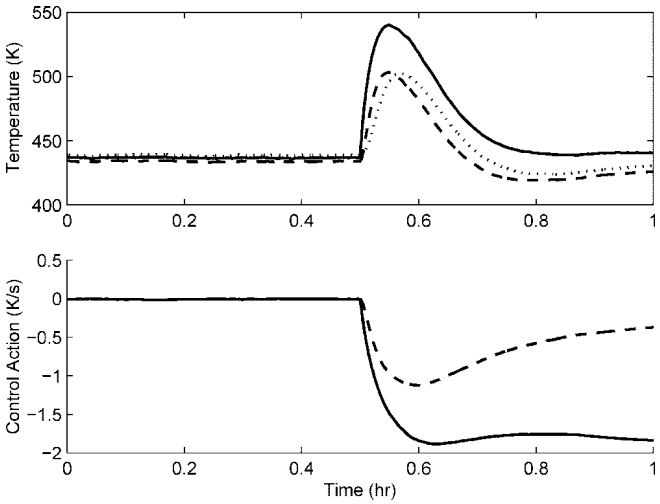

Figure 11. (top) Temperature trajectories for T_1 (solid), T_2 (dashed), and T_3 (dotted) for the system under PI-only control with a failure in d_1 at $t = 0.5$ h. (bottom) Control action requested for the same system for u_1 (solid) and u_2 (dashed).

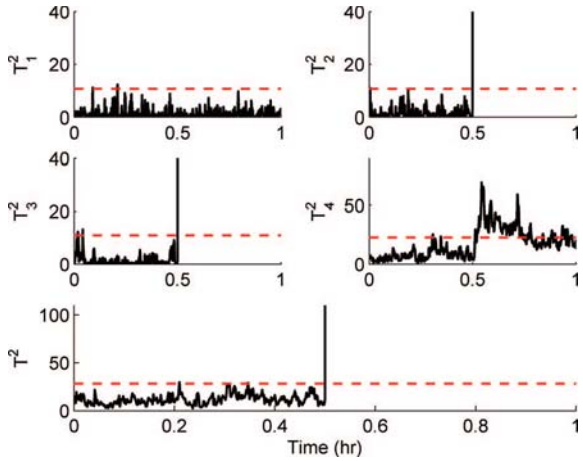

Figure 12. Plots of the T^2 statistic (solid) with the corresponding $T_{\mathrm{UCL}}{}^2$ (dashed) for each of the subsystems and for the full-state vector under nonlinear feedback control with a failure in d_2 at $t = 0.5$ h.

repeated using only a PI controller for comparison. The states were similarly all affected by fault d_1 (see Figure 10), and the control action requested was of comparable magnitude with that of the nonlinear feedback controller (see Figure 11). This demonstrates that the control action requested by the nonlinear feedback control law to enforce an isolable structure is not excessive in this case. For the PI controller, the states of the closed-loop system are all fully coupled, and thus, the state trajectories will all be affected by any fault, making it impossible to distinguish between faults on the basis of process measurements. The simulation with a failure in d_2, below, demonstrates this point.

Figure 12 shows the T^2 results for the simulation in closed-loop operation under the nonlinear feedback controller with a failure in d_2 occurring at $t = 0.5$ h. Note that, although there may be a brief violation of the upper control limit (e.g., at approximately $t = 0.2$ h in Figure 12), this is not declared as a fault nor is it a false alarm since a fault is declared only after a persistent state of failure lasting at least 30 s to avoid such situations. Once the fault is declared around time $t = 0.5$ h, the signature of the system can be determined from the T_i^2 plots that show $W = [0; 1; 1; 1] \equiv W^2$. For the PI-only controller, all of the states were affected as they were in the case with a

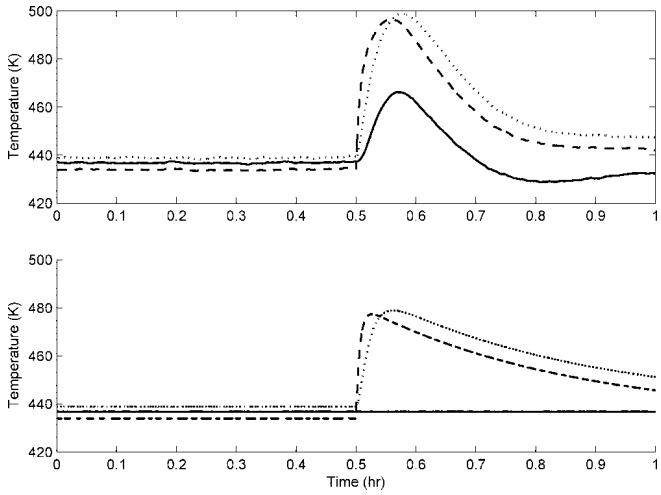

Figure 13. Temperature trajectories for T_1 (solid), T_2 (dashed), and T_3 (dotted) for the system with a failure in d_2 at $t = 0.5$ h under PI-only (top) and nonlinear feedback control (bottom).

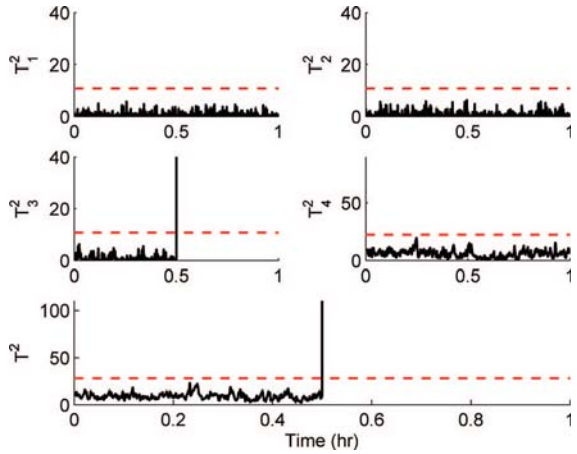

Figure 14. Plots of the T^2 statistic (solid) with the corresponding $T_{\mathrm{UCL}}{}^2$ (dashed) for each of the subsystems and for the full-state vector under nonlinear feedback control with a failure in d_3 at $t = 0.5$ h.

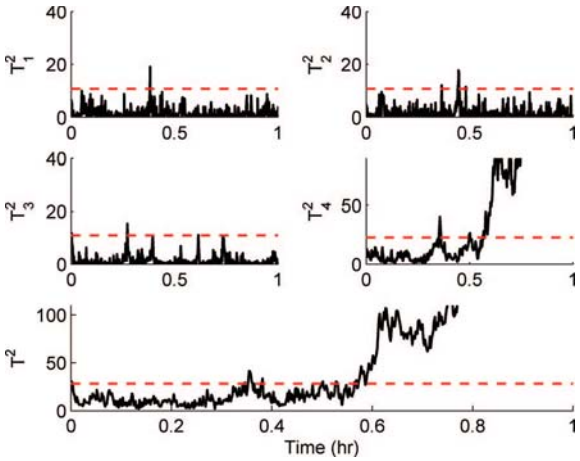

Figure 15. Plots of the T^2 statistic (solid) with the corresponding $T_{\mathrm{UCL}}{}^2$ (dashed) for each of the subsystems and for the full-state vector under nonlinear feedback control with a failure in d_4 at $t = 0.5$ h.

failure in d_1; however, the case with the nonlinear feedback controller designed to enforce an isolable structure correctly shows that T_1 is decoupled from the fault, making it possible to identify. Figure 13 shows a comparison of the temperature plots for the PI-only controller and the nonlinear feedback

Table 4. Fault Sizes and Results from the Monte Carlo Simulation Study

undetected	(count)	false isolation	(count)	correct isolation	(count)
$0 < d_1 < 0.014$	(10)	$0.027 < d_1 < 0.50$	(121)	$0.52 < d_1 < 2$	(369)
$0 < d_2 < 0.022$	(3)	$0.036 < d_2 < 1.49$	(192)	$1.53 < d_2 < 4$	(101)
$0 < d_3 < 0.014$	(10)		(0)	$0.027 < d_3 < 2$	(490)
$0 < d_4 < 0.0012$	(165)		(0)	$0.0012 < -d_4 < 0.002$	(335)

controller to illustrate this point. The plot in Figure 13 (top) shows that, under PI-only control, all of the temperature trajectories are affected (as well as the mass fraction trajectories; however, these have been omitted for brevity), whereas under the nonlinear feedback controller, the unique response can be identified in Figure 13 (bottom) by the fact that the T_1 trajectory is unchanged.

The T^2 plots for the system under nonlinear feedback control with a failure in d_3 are shown in Figure 14. This also shows the expected behavior corresponding to the fault signatures defined in eq 12; that is, the fault affected only the temperature of the flash tank and did not influence the other states. The PI comparison (omitted) showed similar results as before in that all states were affected and a fault could not be isolated based on measured data. Finally, note that, for the system under nonlinear feedback control with a failure in d_4 (see Figure 15), the fault signature only shows that the fault affects the dynamics of the states in $q_4 = \{x_{A1}, x_{A2}, x_{A3}, x_{B1}, x_{B2}, x_{B3}\}$. In this case, the fault signature indicates that there is a fault in d_4 but is unable to distinguish between any of the faults that directly affect the states within this set.

As mentioned in Remark 2, it is possible that faults of intermediate size can be detected but not accurately isolated because of the states being on the threshold of detection and/or possible small gain effects of the directly affected subsystem on another. This was tested in the present model by randomly varying the fault sizes of each of the four faults between 0 and twice the value used in the prior 4 simulations. Each fault was tested with over 500 simulations to determine how large of a fault is necessary to detect and isolate the fault accurately. Table 4 shows the results for these simulations. The results present the range of values for which faults were either undetected, falsely isolated, or correctly isolated as well as the number of simulations for which the faults values fell within the indicated range.

As shown in Table 4, faults d_1 and d_2 had a range of values for which false isolations occurred. This was largely due to the fact that the temperatures had a relatively small gain effect on the mass fractions. This can be compensated for, partially, by increasing the upper control limit of the statistical test for fault detection (T_{UCL}^2 for the full-state vector). While this makes the FDI scheme less sensitive, this reduces the incidences of both false alarms and false isolations.

4. Conclusions

This work has demonstrated the application of a model-based nonlinear controller designed to enforce an isolable structure in the closed-loop system of a multiunit reactor−separator chemical process. Fault detection and isolation were performed using statistical process monitoring techniques and information based upon the imposed closed-loop system structure. This was demonstrated through numerical simulation studies of the closed-loop system in the presence of four different faults. It was shown that, by decoupling faults of interest from certain states, it was possible to achieve unique system responses to each of the four faults, allowing fault isolation based on process measurements only. These results were compared with a conventional PI controller and were thoroughly tested for susceptibility to false isolation through a Monte Carlo simulation study of 500 runs for each of the four fault scenarios.

Acknowledgment

Financial support from NSF, CTS-0529295, is gratefully acknowledged.

Literature Cited

(1) Ohran, B. J.; Muñoz de la Peña, D.; Christofides, P. D.; Davis, J. F. Enhancing data-based fault isolation through nonlinear control. *AIChE J.* **2008**, *54*, 223–241.

(2) Nimmo, I. Adequately address abnormal operations. *Chem. Eng. Prog.* **1995**, *91*, 36–45.

(3) Mhaskar, P.; Gani, A.; Christofides, P. D. Fault-tolerant control of nonlinear processes: Performance-based reconfiguration and robustness. *Int. J. Robust Nonlinear Control* **2006**, *16*, 91–111.

(4) Blanke, M.; Izadi-Zamanabadi, R.; Bogh, S. A.; Lunau, C. P. Fault-tolerant control systems—A holistic view. *Control Eng. Pract.* **1997**, *5*, 693–702.

(5) Zhou, D. H.; Frank, P. M. Fault diagnostics and fault tolerant control. *IEEE Trans. Aerospace Electron. Syst.* **1998**, *34*, 420–427.

(6) El-Farra, N. H.; Gani, A.; Christofides, P. D. Fault-tolerant control of process systems using communication networks. *AIChE J.* **2005**, *51*, 1665–1682.

(7) Mhaskar, P.; Gani, A.; El-Farra, N. H.; McFall, C.; Christofides, P. D.; Davis, J. F. Integrated fault detection and fault-tolerant control of process systems. *AIChE J.* **2006**, *52*, 2129–2148.

(8) El-Farra, N. H.; Christofides, P. D. Coordinated feedback and switching for control hybrid nonlinear processes. *AIChE J.* **2003**, *49*, 2079–2098.

(9) Mhaskar, P.; McFall, C.; Gani, A.; Christofides, P. D.; Davis, J. F. Isolation and handling of actuator faults in nonlinear systems. *Automatica* **2008**, *44*, 53–62.

(10) Qin, S. J. Statistical process monitoring: Basics and beyond. *J. Chemom.* **2003**, *17*, 480–502.

(11) Raich, A.; Çinar, A. Statistical process monitoring and disturbance diagnosis in multivariable continuous processes. *AIChE J.* **1996**, *42*, 995–1009.

(12) Negiz, A.; Çinar, A. Statistical monitoring of multivariable dynamic processes with state-space models. *AIChE J.* **1997**, *43*, 2002–2020.

(13) Frank, P. M. Fault diagnosis in dynamic systems using analytical and knowledge-based redundancy—A survey and some new results. *Automatica* **1990**, *26*, 459–474.

(14) Demetriou, M. A. A model-based fault detection and diagnosis scheme for distributed parameter systems: A learning systems approach. *ESAIM−Control Optim. Calculus Variations* **2002**, *7*, 43–67.

(15) Demetriou, M. A.; Polycarpou, M. M. Incipient fault diagnosis of dynamical systems using online approximators. *IEEE Trans. Autom. Control* **1998**, *43*, 1612–1617.

(16) Kourti, T.; MacGregor, J. Multivariate SPC methods for process and product monitoring. *J. Qual. Technol.* **1996**, *28*, 409–428.

(17) Gertler, J.; Weihua, L.; Huang, Y.; McAvoy, T. Isolation enhanced prinicpal component analysis. *AIChE J.* **1999**, *45*, 323–334.

(18) Yoon, S.; MacGregor, J. Fault diagnosis with multivariate statistical models. Part I: Using steady state fault signatures. *J. Process Control* **2001**, *11*, 387–400.

(19) Westerhuis, J. A.; Kourti, T.; MacGregor, J. F. Analysis of multiblock and hierarchical PCA and PLS models. *J. Chemom.* **1998**, *12*, 301–321.

(20) Bakshi, B. R. Multiscale PCA with application to multivariate statistical process monitoring. *AIChE J.* **1998**, *44*, 1596–1610.

(21) Aradhye, H. B.; Bakshi, B. R.; Strauss, R. A.; Davis, J. F. Multiscale SPC using wavelets: Theoretical analysis and properties. *AIChE J.* **2003**, *49*, 939–958.

(22) Venkatasubramanian, V.; Rengaswamy, R.; Yin, K.; Kavuri, S. A review of process fault detection and diagnosis. Part I: Quantitative model-based methods. *Comput. Chem. Eng.* **2003**, *27*, 293–311.

(23) Venkatasubramanian, V.; Rengaswamy, R.; Kavuri, S.; Yin, K. A review of process fault detection and diagnosis. Part III: Process history based methods. *Comput. Chem. Eng.* **2003**, *27*, 327–346.

(24) Isidori, A. *Nonlinear Control Systems: An Introduction*, 2nd ed.; Springer-Verlag: Berlin−Heidelberg, 1989.

(25) Romagnoli, J.; Palazoglu, A. *Introduction to Process Control*; CRC Press: Boca Raton, FL, 2006.

(26) Tracy, N. D.; Young, J. C.; Mason, R. L. Multivariate control charts for individual observations. *J. Qual. Technol.* **1992**, *24*, 88–95.

(27) Montgomery, D. C. *Introduction to statistical quality control*; John Wiley & Sons: New York,1996.

(28) Demetriou, M. A.; Ito, K.; Smith, R. C. Adaptive monitoring and accommodation of nonlinear actuator faults in positive real infinite dimensional systems. *IEEE Trans. Autom. Control* **2007**, *52*, 2332–2338.

(29) Demetriou, M. A.; Armaou, A. Robust detection and accommodation of incipient component faults in nonlinear distributed processes. In *Proceedings of the 2007 American Control Conference*; New York, 2007; pp 2054−2059.

(30) Demetriou, M. A. Utilization of LMI methods for fault tolerant control of a flexible cable with faulty actuators. In *Proceedings of the 2001 40th IEEE Conference on Decision and Control*; Orlando, FL, 2001; pp 1885−1890.

(31) El-Farra, N. H.; Christofides, P. D. Bounded robust control of constrained multivariable nonlinear processes. *Chem. Eng. Sci.* **2003**, *58*, 3025–3047.

(32) Christofides, P. D. Robust output feedback control of nonlinear singularly perturbed systems. *Automatica* **2000**, *36*, 45–52.

(33) Christofides P. D.; El-Farra, N. H. *Control of Nonlinear and Hybrid Process Systems: Designs for Uncertainty, Constraints and Time-Delays*; Springer: New York, 2005.

Received for review November 14, 2007
Revised manuscript received February 27, 2008
Accepted February 29, 2008

IE071548I